Coherent beam combining strategies for highenergy and high-repetition rate lasers dedicated to inertial nuclear fusion applications

Pierre Lebegue, Marie Froidevaux, Jonas Benjamin Ohland, Cyril Rapeneau, Doina Badarau, Joanna de Sousa, Loïc Meignien, Ivan Doudet, Nolan Chan, Benoit Wattellier, et al.

Coherent beam combining strategies for high-energy and high-repetition rate lasers dedicated to inertial nuclear fusion applications

PIERRE LEBEGUE[1,2], MARIE FROIDEVAUX,[2] JONAS BENJAMIN OHLAND,[2,3] CYRIL RAPENEAU,[2] DOINA BADARAU,[2] JOANNA DE SOUSA,[2] LOÏC MEIGNIEN,[2] IVAN DOUDET,[4] NOLAN CHAN,[4] BENOIT WATTELLIER,[4] PATRICK AUDEBERT,[2] DIMITRIS PAPADOPOULOS,[2,*] FRÉDÉRIC DRUON[1]

1. Laboratoire Charles Fabry, Université Paris-Saclay, Institut d'Optique Graduate School, CNRS, Palaiseau, France
2. LULI, CNRS, École Polytechnique, CEA, Sorbonne Université, Institut Polytechnique de Paris, Palaiseau, France
3.GSI Helmholtzzentrum für Schwerionenforschung, Planckstraße 1, 64291 Darmstadt, Germany
4. Phasics S.A., Route de l'Orme des Merisiers 91190, Saint-Aubin, France

†These authors contributed equally.
**dimitrios.papadopoulos@polytechnique.edu*

Abstract: Spatial Coherent Beam Combining (CBC) strategies are particularly promising for lasers dedicated to nuclear fusion applications in the purpose of developing high-energy and high-repetition-rate lasers. Let us examine their potential application to high-energy, large-size beams with repetition rates that preclude phase correlation between subsequent pulses. Both passive and active CBC approaches are investigated in this study to identify the most appropriate and effective strategy for large-aperture, high-energy laser amplifiers. Specific experiments have been conducted to validate promising architectures for lasers dedicated to inertial confinement fusion (ICF) applications. Based on these experimental results, examples of suitable and well-adapted setups are proposed.

1. Introduction

The pursuit of Inertial Confinement Fusion (ICF) has garnered significant international attention, particularly following recent demonstrations of net energy gain at the National Ignition Facility (NIF), achieving a 1.5x gain [1] and, subsequently, a 4.13x gain [2]. In response to the escalating interest in inertial fusion energy (IFE), substantial efforts in high-energy laser development have been dedicated to creating novel laser sources capable of meeting the broad specifications of an "ideal" laser for ICF applications.

Various schemes and configurations have been proposed to achieve these demanding requirements. These include gas laser systems emitting directly in the ultraviolet (UV) spectrum [3], solid-state lasers with lower energies in the 100 Joule range that are incoherently combined on the target, following architectures such as the "Star Driver" concept [4], and more futuristic approaches like fiber laser-based architectures that combine tens of millions of individual 10-100 mJ fiber sources [5]. While each of these approaches has its own merit, and research worldwide continues in these fields, the dominant research effort is focused on the development of laser systems capable of kilojoule energies at 10 Hz repetition rates with ICF laser sources based mainly on the Nd:glass material. This choice is largely driven by two factors: the imperative to simplify the overall ICF facility, minimizing the number of laser sources to 1000-2000 at maximum, and the requirement of a material that, even if problematic in terms of thermal management, can still provide some bandwidth

potential in the range of 1-2%, still valuable for the stability and efficiency of the ICF interactions [6].

Kilojoule-class laser systems based on flashlamp-pumped Nd:glass sources have been extensively employed as fundamental "building blocks" in numerous facilities worldwide, including the NIF and the Laser Mégajoule (LMJ) [1,7]. Despite their widespread use, these sources are severely limited in repetition rate, offering only a few shots per day or, at best, approximately one shot per hour. Recent advancements, however, have leveraged the combination of liquid or gas cooling techniques with multi-slab active elements pumped by laser diodes [8-11]. These innovations have pushed the repetition rate of high-energy lasers to approximately one shot per minute for kilojoule-class systems [12] and 10 Hz for 100-200 Joule sources [13]. For these state-of-the-art developments, it has become evident that the average power barrier of 1-2 kilowatts represents the primary bottleneck hindering further progress. A breakthrough innovation is clearly needed to enable the decisive step forward towards achieving the "ideal" laser sources for future ICF-based power plants. While ongoing research focuses on further development of efficient cooling techniques, new materials, and optimized pumping schemes, we assert that coherent beam combination (CBC) is also a valid and complementary approach with strong potential towards the development of kilojoule-class high repetition rate systems.

In this work, we investigate in detail a potential kilojoule-class system capable of operating at 10 Hz repetition rate, based on the coherent combination of lower energy systems that are technologically readily available in the 10 Hz repetition rate regime. While CBC has been extensively studied mostly in the context of low-energy fiber-based systems [14-17], its applicability to high-energy systems has been primarily theoretical until recently. High-energy laser sources present two significant specificities relative to their real capacity for CBC: first, their large beam aperture, which is subject to non-negligible spatial wavefront instabilities, second, the low repetition rate for the servo-loop leading to on-shot erratic, unpredictable, potentially-violent and excessively-fast piston and wavefront distortion during the pump cycle (either flash lamp or diode pumped). Based on our recent works demonstrating for the first time the applicability of CBC methods for 100 Joule-class systems [18] and our thorough investigations into limiting on-shot effects towards further scaling to the kilojoule level [19].

More specifically, this article first presents a study on passive coherent beam combining (CBC), based on what is now considered a realistic and technologically mature building block for laser systems operating in the 20–30 J range at 10 Hz (corresponding to average powers of 200–300 W). We demonstrate that this passive CBC architecture can reliably achieve energy levels of up to 100 J. Following this, we present a novel experimental study proving that such beams can also be actively combined. From those considerations on both passive and active CBC, we propose a realistic architectural scheme capable of delivering 1 kJ at 10 Hz, thereby addressing the key challenges and requirements of ICF and IFE applications.

2. Passive CBC

As mentioned above the use of (CBC) can play a significant role in the area of large-scale high-energy laser development. However, up to now, experimental demonstrations of CBC have primarily involved small size beams, as the energy levels were relatively low even with bulk materials [20,21]. In such systems, the spatial homogeneity of the beam was not a critical issue, thereby reducing the phasing problem to a phase-piston control. Moreover, the lasers involved typically operated at high repetition rates, allowing access to feedback loops operating in the kHz regime without encountering strong and unpredictable phase instability between shots [14-17,21-23]. In this context, the main new questions to be addressed concern the potential spatial issues of large-aperture beam combining and the absence of phase correlation between subsequent pulses, which are specific to Joule-level laser chains. One

way to overcome the low-repetition rate bottleneck is to use the passive CBC since it does not need feedback loops requiring high repetition rate measurements.

To this end, we propose to study CBC with a robust, easy-to-implement architecture using amplifiers embedded in a Sagnac-interferometer geometry applied to multi-cm-size bulk gain media. This passive CBC indeed requires no servo-control, which renders this approach particularly suitable for low repetition rate systems, and is based solely on polarization separation and recombination, making it easy to implement [18]. The input pulse is split into two beams, each carrying half of the energy. Each beam can then be amplified separately, thereby reducing the fluence on the amplifier media and minimizing non-linear effects such as the B-integral and subsequent deleterious hot-spots. As a beneficial outcome, this enables us to operate further away from the damage threshold or alternatively reduce the diameter of the amplifiers from the point of view of potentially increasing the repetition rates. Once the two beams are amplified, they are combined in phase to form a single beam. In the Sagnac interferometer, the two split pulses automatically share the same optical path but propagate in opposite directions, leading to robustness against spatial imperfections in the optical path distance. In addition, this configuration can be implemented on existing laser chains and does not require exotic components (Fig 1).

In this section, we will demonstrate how this concept can be scaled to 100-J levels, supported by preliminary results obtained from recent experiments conducted on an energetic nanosecond laser chain based on Nd:glass. Our objective is to address spatial issues within a 4-cm-diameter beam system, thereby facilitating the application of CBC to hundred-joule-class laser chains. This work allows us to identify where spatial issues become critical and highlight the crucial bottlenecks that have been considered. From the perspective of extending this concept to high wall plug efficiency, high-energy systems with higher repetition rates, we will propose architectures that optimize the laser-induced damage threshold (LIDT) and energy extraction saturation. Finally, we will explore how these simple architectures can be extended to incorporate more than two combined amplifier modules, and discuss the associated increase in complexity while keeping the high beam quality.

The various technical challenges of passive-Sagnac CBC are summarized in Figure 1, showing architectures with different gain media geometries to optimize the thermal dissipation and to enable amplification at a shot rate of up to 10 Hz [24-26]. A “double-pass Sagnac interferometer” (Fig. 1 bottom) can also be created by adding a quarter-wave plate and a 0° plane mirror at the output. The two counter-propagating beams invert and make an inverse round trip. This setup increases the gain for a given amount of amplifying medium. Note that polarization-sensitive amplifiers (such as slabs at Brewster angle) can also be used. To incorporate them into a Sagnac interferometer, one must either complicate the polarization management [16] by integrating additional wave plates and/or actives elements, either by replacing the PBS by a 50:50 beam-splitter that preserve the polarization. In this last case, to select the right output of the Sagnac interferometer, it is then possible to do it by slightly adjusting vertically one of the mirrors of the interferometer, as observed in [18].

In designing the Sagnac interferometer for high-energy applications, it is crucial to consider the LIDT of the optics. Few points have to be considered in their conception such as the propagation lengths to avoid overlapping of the contra-propagative beams in the amplifiers and even more crucially the Sagnac beam splitter/combiner element which receives the full energy. From this perspective, the polarizing beam splitter should be used at a large angle ideally exceeding 60° to increase the beam section on its surfaces. For the optics employed in the double-pass configuration also seeing the combined-beam fluence -optics consisting in a half-wave plate and a Polarizing Beam Splitter (PBS) used for extraction-, several strategies can be considered. These include integrating a telescope to enlarge the beam or utilizing half-wave plates with higher LIDT (with the potential use of off-plane mirrors to rotate the linear polarization) in conjunction with a polarizer set at an angle greater than 60°.

The challenges related to the large beam size primarily also concern the number of mirrors used in the interferometer, which should be odd to ensure that the same part of the input beams recombines. However, the large beam amplification in a Sagnac involves a spatial symmetry in the amplification of the two different polarization states counter-propagating in the interferometer. This is illustrated in Figure 2. By misaligning a Sagnac mirror to create on purpose some fringes we can use the shearing technique to retrieve the potential phase lateral asymmetry between the two counter-propagating beams on the amplification process. This point in our experimental example using flash-pumped Nd:glass leads to only a marginal 1% of combination defect. Finally, in order to systematically avoid amplification asymmetry, the solution of double pass Sagnac amplifier can be proposed.

Additional tests could be conducted to validate the architecture. The first test concerns potential backward injected beams. In the single-pass Sagnac configuration, the value was measured to be below 0.1% in the test case using flash-pumped Nd:glass amplifiers [18]. Such intense back-scattered light can easily be handled using conventional isolation methods such as Pockels cells or Faraday isolators. The second point involves the polarization state at the output of the signal, which corresponds to the efficiency of the beam combining since dephasing between the two contra-propagating beams indeed leads to polarization degradation. The CBC efficiency measured in our test bench has been measure around 92 % [18]. In the one pass Sagnac configuration this polarization does not impact the output energy but may impact polarization-dependent post amplifiers. Moreover, the CBC efficiency loss is particularly important to evaluate in the double pass configuration in order to optimize the optical isolation in the front of the amplifier.

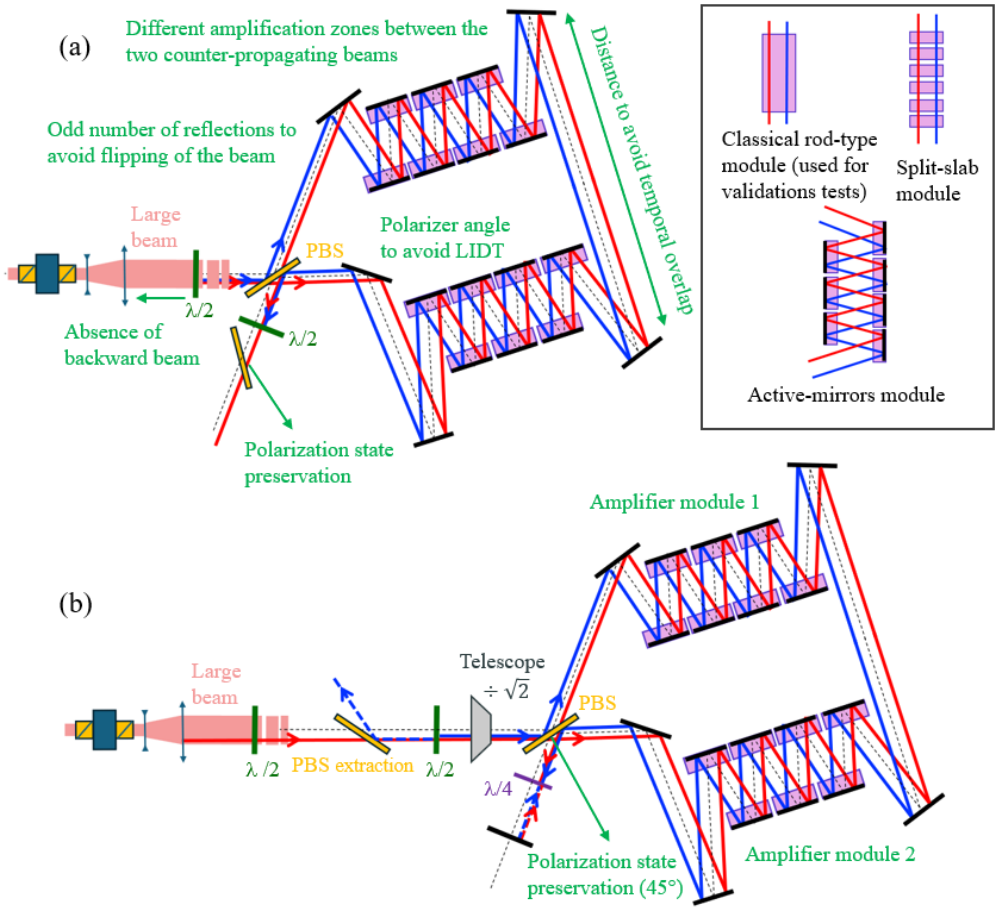

Figure 1: Example of a passive CBC setups ((a): in single-pass, (b): in double-pass), highlighting specific issues (indicated in green) associated with high-energy beam amplification. The blue and red paths represent the two different polarization states counter-propagating within the Sagnac interferometer. Inset: example of amplifiers modules including the ones adapted to the heat-removal for high-repetition-rate operation. (In the second setup, the final half-wave plate —that rotates the polarization by 90°— can be replaced by two mirrors at 45° in order to reduce the fluence on their surfaces.)

Taking these considerations into account and based on the preliminary experimental results obtained, we can propose a simple architecture as shown in Fig.1 in order to reach the 100 J level with 4-cm-diameter beams and a LIDT of 4 J/cm². Considering a stored energy of 82.4 J per amplifier, a small signal gain of 3.16 per amplifier module and assuming a saturation fluence of 4.5 J/cm², the double-pass-Sagnac-configuration (bottom row in Fig.1) amplifier can produce up to 120 J with a relatively modest beam diameter for an injected energy of 2.5 J as shown in figure 3. This architecture offers several advantages. Firstly, it facilitates a reduction in the LIDT by separating the optical paths and mitigating the effects of hot spots, as the recombination process tends to average the beam profiles. It is important to note that these different paths do not imply discrepancy in the CBC process which is estimated to be less than 1% in our case, see Fig. 2. Secondly, in a cascade amplifier configuration—better suited for high-repetition-rate amplifier cooling—the counter-propagation within the Sagnac interferometer reduces the impact of gain saturation. As illustrated in Figure 3, the Frantz-Nodvik model [27] which has been validated in the Sagnac configuration [18], demonstrates

that this setup enhances extraction efficiency and better preserves the temporal shape of the pulse, thereby requiring less pre-compensation.

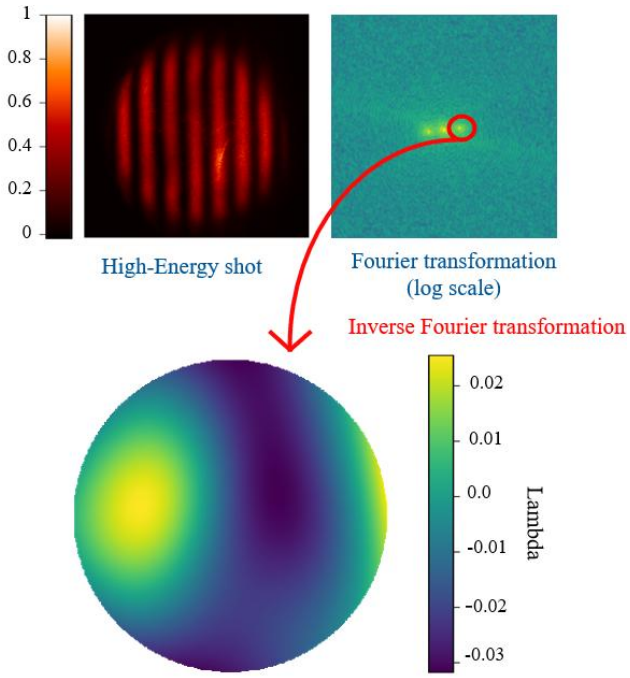

Figure 2: Experimental measurement of the impact due to the different amplification paths between the two contra-propagating beams in a single-pass Sagnac amplification process.

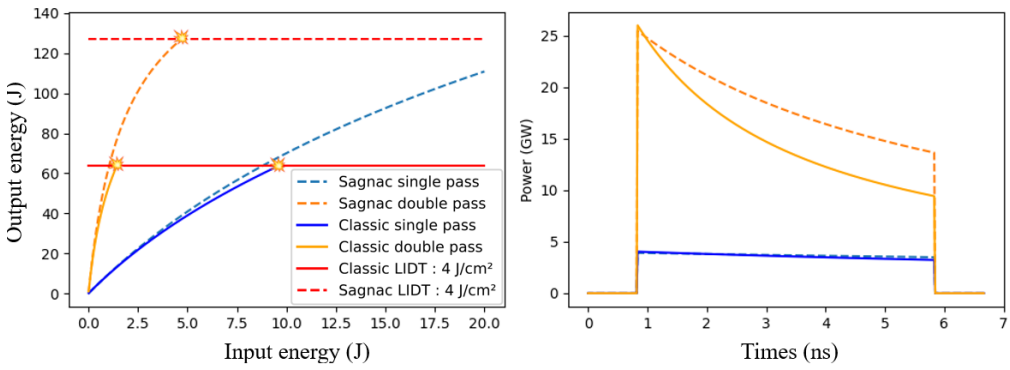

Figure 3: Extracted energy (on the left) and temporal saturation (on the right) for different configurations simulated using Frantz-Nodvik model [27]: in a "typical" configuration (dash lines) - simply going through the two consecutive amplifier modules - and in Sagnac configuration (solid line) for a single pass (blue lines or a double pass - making a round-trip (orange lines). Temporal profile (on the right) showing the difference of gain saturation between the classical and the Sagnac configurations.

To go further, since the interest of passive CBC is particularly convenient for low repetition rate large-diameter beams, the question of extending the simple 2-amplifier module combination to a Sagnac interferometer and to even higher number of Sagnac amplifiers

modules is interesting. Indeed, it is feasible to extend passive CBC using the same principle of employing interferometers —specifically, here, Michelson geometry interferometers— to combine 2^n amplifier modules, as illustrated in Fig. 4. In this configuration, the initial beam is subsequently divided in 2^n and each beam in passing to all the 2^n amplifier modules. The optical pass of each beam is then strictly similar to the other. However, it is simple to demonstrate that these 2^n-beam passive CBC configuration is clearly not optimized for larger beam diameters. Indeed, as mentioned before the weak point in the passive CBC is the PBS combiner seeing the total fluence. Concretely, in the point of view of minimizing the amplifier diameter to increase the repletion rate, passive CBC is still working but has a strong cost on its complexity since at each step from 2^{n-1} to 2^n amplifiers two telescopes have to be added to expand the beams —by a $\sqrt{2}$— before the n^{th} beam-splitter ("PBSn" in fig. 4 which by the way is also larger than the previous optics and consequently the amplifiers). Incorporating telescopes into the Michelson interferometers is particularly challenging, as both telescopes must exhibit identical characteristics from an interferometric perspective, including optical spatial aberrations. At each step, one has to add (to the optics corresponding to two 2^{n-1}-beam CBC systems) two beam expenders together with a larger PBS and three larger quarter-wave plates, which make the system complexity drastically increasing at each step.

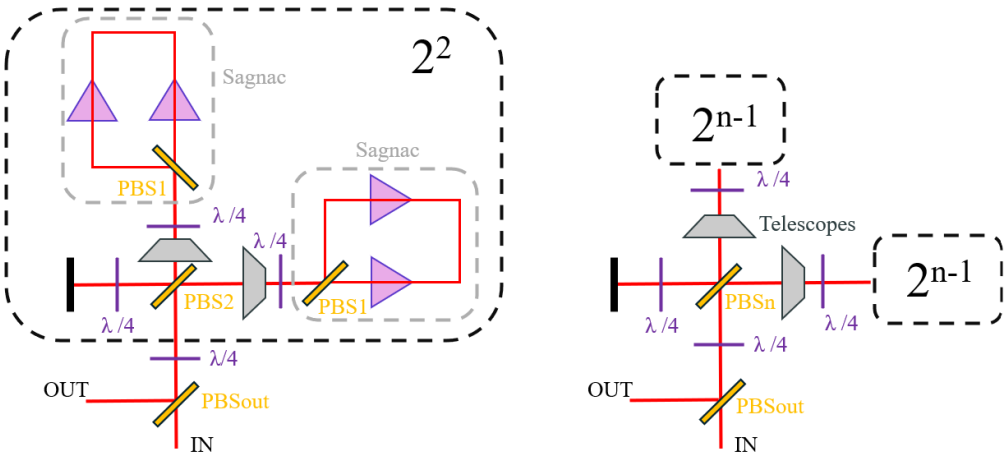

Figure 4: General setup for 2^2 amplifiers passive CBC (left) and the generalization for 2^n amplifiers passive CBC (right), by induction. PBSn stands for polarization beam splitter on the n^{th} step.

In conclusion, the passive CBC technique is relatively straightforward to implement for two amplifiers modules with moderate diameters, typically around 4 cm, to achieve energy levels of approximately 100 J. This method is particularly suitable for combining beams in the absence of phase correlation between subsequent pulses and is especially effective in managing gain saturation. However, its extension to more than two blocks becomes increasingly complex and rapidly loses efficiency [28]. Therefore, to achieve higher energy levels, the use of active CBC appears to be a more pertinent option.

3. Active CBC for high energy

Active CBC offers the capability to merge multiple beams that traverse different paths and amplifiers [14,16,20], known as sub-beam lines. Since these paths are independent, it is feasible to incorporate a beam expander before the recombiner. This setup, unlike passive combination, allows for significantly greater scalability in number of combinable sources.

However, this advantage comes with the challenge of actively compensating for the relative phase shift of each sub-beam line in real-time, which remains an unresolved issue in high-energy, large-aperture, and slow-repetition-rate laser chains.

There are four primary methods to recombine beams (Figure 5):

- By Polarization [14,15,17,21]: Efficient and relatively straightforward for combining beams. However, it may become increasingly complex and space-consuming when scaled up to many beams, as it typically operates pairwise.
- By Aperture [14,15,22,23]: Well suited for combining many beams, this method can suffer from reduced efficiency due to the limited filling factor, particularly when using Gaussian beam profiles. To optimize spatial coverage and minimize losses, beams with top-hat intensity profiles and square or hexagonal shapes are preferred, as they enable efficient spatial tiling without gaps.
- By Diffractive Optical Elements (DOE) [14,15]: Highly efficient in theory, even with many beams. However, manufacturing sufficiently large DOE gratings with good LIDT and capable of handling average power remains challenging.
- By Brillouin Effect [29]: Difficult to set up and imposes several constraints in terms of temporal fidelity [30]. It is also incompatible with broad spectral ranges (more than 100 MHz), which can be a severe limitation for fusion applications.

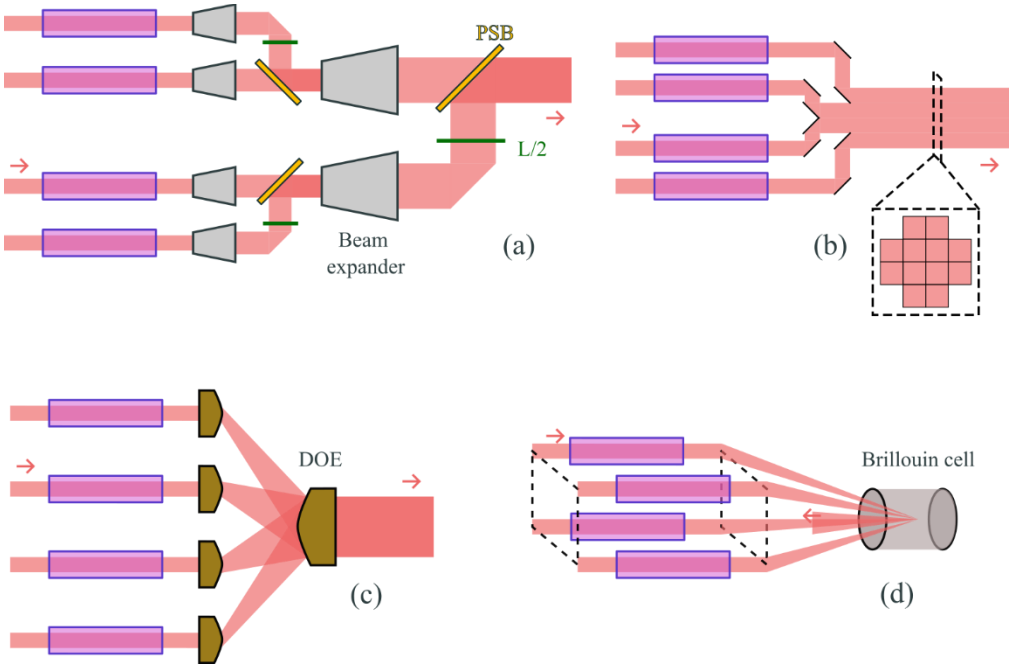

Figure 5: Principle demonstrating multi-beam recombination schemes. (a) by polarization, (b) by aperture, (c) by DOE and (d) by Brillouin effect.

Given that active CBC is suitable for combining numerous laser chains, it is advantageous to use it in the final amplification stage. This approach ensures that no amplifier needs to handle the final beam diameter, thereby avoiding the slow cooling problems of large amplifiers that impose the low cadence of kilojoule chains.

For inertial confinement fusion, it is reasonable to consider combining a large number of lasers, each delivering several tens joules at a repetition rate of tens of hertz. Such lasers would require multi-centimeter diameters, introducing a significant difference from the

current state-of-the-art in active combination. First, in this regime, phasing is no longer a "simple" 0D piston correction; instead, additionally full 2D wavefront control across the entire aperture becomes necessary. Furthermore, unlike demonstrations reported in the literature, the laser alone does not have a sufficiently high repetition rate to allow for shot-to-shot feedback, given that the cadence is much lower compared to the timescale of pumping and thermal diffusion (pumping which typically range from a few microseconds to a few hundred microseconds).

To address these issues, one potential strategty consists in using a continuous wave (CW) probe laser with the same beam size that co-propagates with the main beam. When employing a feasible separation strategy, *e.g.* a slightly detuned central wavelength and dichroic mirrors/filters [31], the probe beam grants insight into the spatial dephasing right up to the amplification of the pulse. The probe wavelength can also be taken outside the amplification peak to minimize energy dynamics and simplify diagnosis. The idea is to probe each sub-beam line this way, designate one as the main sub-beam line (the master), and have all the others (the slaves) phase locked onto the master using sufficiently fast adaptive optics (AO) systems. The two main parameters to extract from the probe are the relative phase delay (piston) and the differential wavefront. To measure these parameters, we could use shearing interferometry as described in Fig. 6.

The cumulative evolution of wavefront distortion following a shot sequence on such a laser chain is already well understood and has been previously studied. The aberrations introduced by the effect of the flash increase steeply and relax over a period of a few tens of minutes. Nevertheless, a cumulative thermal load is observed, causing the beam quality to continuously vary over extended times of operation [32]. This information primarily informs us about thermalization and, consequently, about the operating cadence. In terms of coherent combination, we are primarily interested in the on-shot aberrations, *i.e.*, aberrations arising during the pumping process, as the pulse is being amplified, occur on a timescale of tens of microseconds. Unfortunately, except from very few preliminary works [33], there is a lack of documentation on the precise characterization and understanding of these on-shot-induced aberrations on large energy scale laser chains. The characterization of such effects is challenging and requires complex diagnostics capable of measuring the wavefront with high temporal resolution and over a wide dynamic.

In this paper, we present the results of a recent experiment conducted on a large-scale laser facility (the HERA laser facility at LULI, France), where we used a spectrally shifted continuous beam at 1064 nm to probe the 2x200 J Nd:glass flash-pumped-based laser chain operating at 1053 nm. Our setup (fig. 6) allows the continuous monitoring of the relative phase distortions (both piston and wavefront) before, during, and after the amplification process, since in our case the Kramers-Kronig phase shift [34] between the two wavelengths is negligible and the amplification in each sub-beam line is similar. For the acquisition we employed a fast wavefront sensor with an adapted region of interest (ROI) to increase the acquisition speed (SID4-kHz with 576x184 pixels and an exposure time of 10 µs at 61 kHz) in order to characterize the evolution of the wavefront evolution of each sub-beam line. The spatial interference between these two beams is also measured to retrieve the piston needed for active CBC prospect. The laser chain and the diagnostic apparatus are shown in fig. 6.

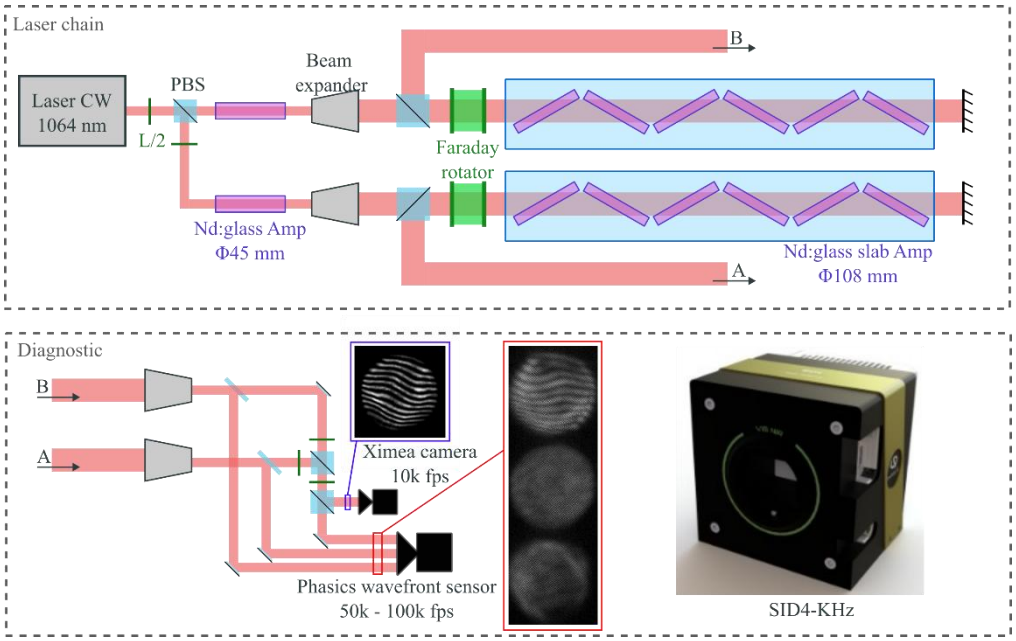

Figure 6: Experimental setup of the on-shot aberration measurement at the HERA LULI laser facility. The laser chain is probed with a CW laser at 1064 nm (300 mW). At a certain point, the laser chain splits into two sub-beam lines (A and B), each comprising a 45 mm Nd:glass rod amplifier and a 108 mm Nd:glass slab amplifier. Each laser line then passes through a telescope to reduce the beam from 90 mm to 3.5 mm for diagnostic purposes. Two sensors are used: 1) A SID4-kHz simultaneously measures the wavefront of each sub-beam line A, B, and their interference; 2) a fast camera (Ximea XiB64 CB013MG-LX-X8G3-TG) serves as a comparison witness, observing only the two beams interference pattern.

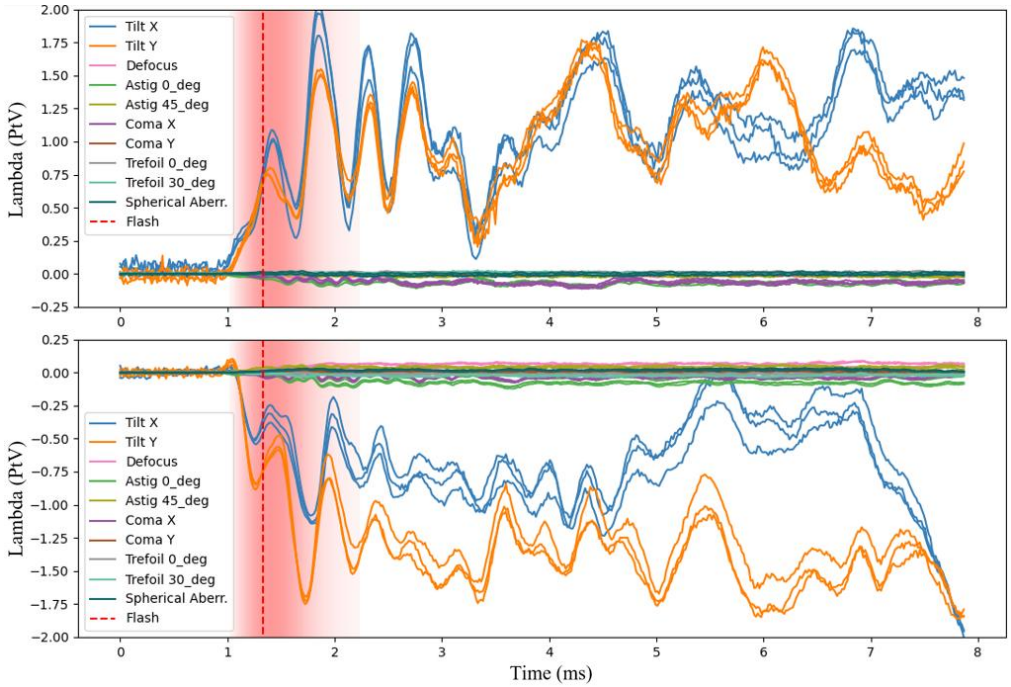

Figure 7: Wavefront decomposition for three flash pumping events probed with the 1064 nm CW laser for the two sub-beam lines: A (top) and B (bottom). Fluorescence due to the flash pumping follows the intensity of the red shading. The amplified laser pulse at 1053 nm typically arrives at the time indicated by the vertical red dashed line (maximum of fluorescence). Wavefronts are self-referenced just before the start of the flash. Three different shots spaced about 20 minutes apart are plotted on the graphs (lines of the same color)

The results shown in Fig. 7 have been obtained with the setup described in Fig. 6. To analyze the results, we can first focus our attention on the evolution of the wavefronts of each individual beam. To achieve this, we use the wavefronts recorded just before the pumping pulse as a reference, in order to eliminate the influence of static aberrations due to alignment and slow dynamic aberrations like atmospheric and thermal turbulence which are common in large-scale facilities. As shown in Fig. 7, the wavefront distortions do not vary significantly above the noise level during the millisecond preceding the flash, confirming the slow temporal variation of these environmental effects. Indeed, we observed, between shots, varying wavefront distortions (below 100 Hz) due to atmospheric and thermal fluctuations that can be considered slow compared to the pumping flash duration. These fluctuations are not considered in our study but can play an important role. It as has been shown recently their correction is possible with readily available technologies [31].

Regarding the fast on-shot effects, we observe that aberrations are mainly tilts along the X and Y axes. A significant, though much lower, amount of coma and astigmatism is also observed, while other aberrations (defocus for instance) remain within the measurement noise. Three distinct temporal behaviors can be identified: before the flash, aberrations slowly fluctuate (< 100 Hz); during the flash, perturbations rapidly grow (rates between 1 kHz to 10 kHz) but relatively reproductible (and then potentially predictable); and after the flash, a relaxation era with fluctuations that are still violent (1 kHz to 100 kHz) but gradually shifting slowly toward erratic behavior.

For active coherent combination, our amplified 1053 nm laser pulse of a few nanoseconds only experiences the aberrations introduced at the peak of fluorescence intensity (red dashed line in Fig. 7). The first challenge is to ensure the same wavefront on both beam lines at that instant. Since, for our flash-pumped-amplifier system, the measurement gives 1-λ-shift introduced in approximately 375 µs, this would correspond to a corresponding bandwidth of 55 kHz for the feedback loop in order to correct the phase with a precision of λ/20. A phase precision of λ/20 is a good trade-off target [35], since it is attainable with standard phase-shift control and corresponds to a combination efficiency of about 99% for 2 beams or about 91% for 12 beams. Two approaches are possible. Either a device with sufficient bandwidth can correct the few more significant terms of the wavefront (mostly the tilts) in real-time, or taking advantage of the reproducibility of the system (well designed and characterized), to pre-compensate the fast phase shift few milliseconds before the flash-pumping. If the latter seems more realistic given the state-of-the-art in large-diameter actuators, both methods can be used to ensure greater precision while reducing real-time actuator bandwidth. Other on-shot high-order aberrations are negligible and can be ignored as long as alignment aberrations are already effectively corrected.

The second challenge concerns the differential piston phase between the two beamlines. To retrieve this, analyzing the interference fringes between the two beams is essential. The results shown in Fig. 8 illustrate the dynamic evolution of a central portion of the fringes pattern leading to the differential wavefront between A and B over time. Piston can be extracted as well as the tilt along the selected band axis. However, in this part we focus on the piston analysis which corresponds to the shift in the fringe pattern and must be tracked frame by frame, which is feasible only if the temporal sampling frequency exceeds the time required for the system to shift by λ/2. Regarding the analysis of the results, we find similar outcomes to those of the beam tilts analysis, characterized by three periods: before, during, and after the

flash. At the peak of fluorescence, we observe approximately a piston of λ/2 introduced during 100 µs, then necessitating feedback at 100 kHz to adjust to λ/20.

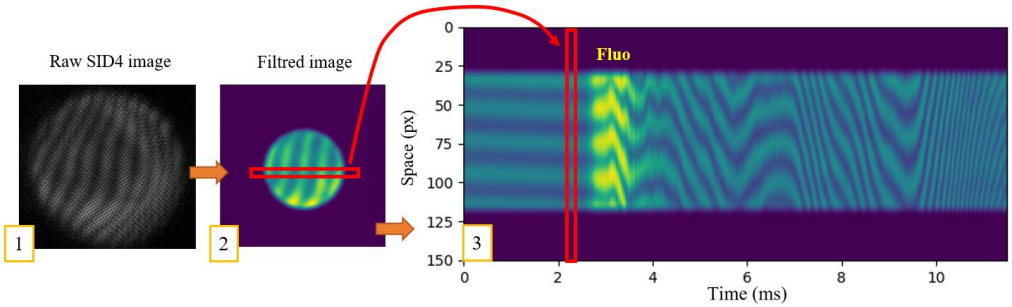

Figure 8: Data processing and piston analysis. Measurements were made with the SID4-kHz and the setup described in Fig. 6. The direct result of the 4-wave interferometer is presented in sub-figure 1. After spectral filtering and cropping, the processed image is shown in sub-figure 2. A few pixel rows are selected and averaged before being stacked frame by frame in sub-figure 3. The abscissa axis represents time, and the vertical axis represents space (fringe along an axis).

We can then conclude from our measurements that efficient CBC requires global differential wavefront correction, mainly by controlling both the piston phase difference and phase tilts of the two sub-beam lines. The focus here is on the component of the wavefront that evolves during the pump flash. As shown in Fig. 8, analyzing the fringes pattern over a reduced pupil appears to be both feasible and well-suited for retrieving the piston phase. This approach also allows us to disregard systematic fringes distortions that arise — in our case — from alignment challenges particularly within the high-numerical-aperture reducing telescopes used in the diagnostic setup. Moreover, since the selected part contains no higher-order aberrations, we can reasonably equate the local tilt to the global tilt and the piston is easy to retrieve.

A strategy for efficient active CBC with large beams can thus emerge. For practical implementation, the feedback loop should be divided into three distinct actions:

- slow wavefront distortions caused by environmental effects should be corrected independently on each beamline using adaptive optics with dedicated feedback loops. This will prevent any excessive tilt or aberration that could distort the fringe pattern along the selected axis for analysis. Such distortions —causing fringe rotation or drastic variations in the fringe spacing—would otherwise limit the accuracy of subsequent measurements.
- The piston and tilts, which are the mains phase distortions occurring during pumping, could be significantly compensated by implementing precise phase pre-compensation based on the predictable nature of those effects. It should be noted that, even if the amplitude of the higher-order aberrations appears negligible, they can also be pre-compensated if necessary.
- The on-shot phase piston is most critical aberration for CBC efficiency. It can be fully or partially (in addition to pre-compensation) processed via an accurate feedback loop operating at around 100 kHz. For this phase piston analysis, only one axis can be considered and line camera can be used to increase the live performance speed instead of a regular 2D camera. The feedback bandwidth can be obtained with Field-Programmable Gate Array (FPGA) board coupled with a

phase modulators placed at the beginning of each sub-beam line to take advantage of small components that achieve sufficient processing speeds.

4. Design proposition for 1kJ at 10 Hz

To meet the requirements of ICF and IFE as described in the introduction, the goal is to create a laser chain capable of delivering laser pulses of a few nanoseconds with temporal profiling, achieving energies up to one kilojoule at a repetition rate of 10 Hz, and having a spectral width up to a few tens of nanometers. To achieve temporal and spectral profiling as well as good contrast, it is common to use a Master Oscillator Power Amplifier (MOPA) architecture. The critical point lies in the final amplifiers responsible for energy extraction, which determine the chain's repetition rate through their thermal management. Various materials can be used, such as Nd:glass [7,11,25,26,32], Yb:YAG [8,13], etc. The choice of material affects the central wavelength, spectral width, gain, and saturation fluence. Different pumping methods can also be employed, such as flashlamp, light-emitting diode (LED) [36], or laser diode [8,10,13], which mainly influence efficiency, operational cost, and thermal load on the system. Additionally, the geometry of the amplifiers must be optimized for maximum efficiency and repetition rate, for example, using slab or pseudo-active mirror configurations (Fig. 1). Finally, the number of amplifier elements must be adjusted to achieve the desired raw gain. The chain is intrinsically limited by LIDT and B-integral. For a given beam area; for example, with optics of 4 to 5 cm in diameter, the maximum energy to ensure an LIDT below 4 J/cm² is 50 to 78 J with standard classical amplification and can be doubled using passive CBC as described in section 2, reaching up to 157 J. For the remainder of this section, we consider the use of amplification modules based on passive CBC capable of amplifying from 1 to 100 J at 10 Hz. An explicit example of an architecture based on Nd:glass is described in section 2. Another advantage of this architecture is the ability to build a kilojoule laser using only 40 mm-diameter amplifier mediums, thus making it possible to use certain materials (in particular crystals) that are currently extremely difficult, if not impossible, to manufacture in the dimensions without lattice defects, but would be required for direct amplification up to the kilojoule (~20 cm diameter for a 4 J/cm² LIDT).

To achieve 1 kJ with an active CBC efficiency of 80 to 90%, it would be necessary to combine at least 11-to-12 100-J-class laser chains. The exact required performance depends on the specific needs and is influenced by the recombination technology. It is more suitable to combine an odd number of beams with DOEs, hence 11 beams. A configuration with 12 beams in a square arrangement, as described in Fig. 5, may be appropriate for tiling. Polarization recombination is adapted to combine powers of 2 beams, thus 8 or 16 for performances slightly below or above the kilojoule. However, this last over-dimensioned architecture can be used as an advantage for chain maintenance, since polarization recombination also offers the possibility of enabling only certain sub-beam lines by reorienting the half-wave plates, for example, 12 out of 16 sub-beam lines to reach the kilojoule. This strategy ensures performance even during chain maintenance, which can be very advantageous for continuous use in energy production through ICF. Recombination by DOE and tiling does not offer this robustness, and their performance is significantly degraded when one sub-beam line is stopped. Nevertheless, replacement devices can be implemented.

The total size of such a system depends on the requirements and technologies involved. For example, the size of an amplifier based on Sagnac architecture depends directly on the pulse duration to avoid temporal overlaps. It is appropriate to estimate 1 to 2 m² footprint for systems developed for pulses of a few nanoseconds. Transport and the recombination method also contribute to the overall size. It would be reasonable to estimate a total overall footprint of 50 m² for 1 kJ system.

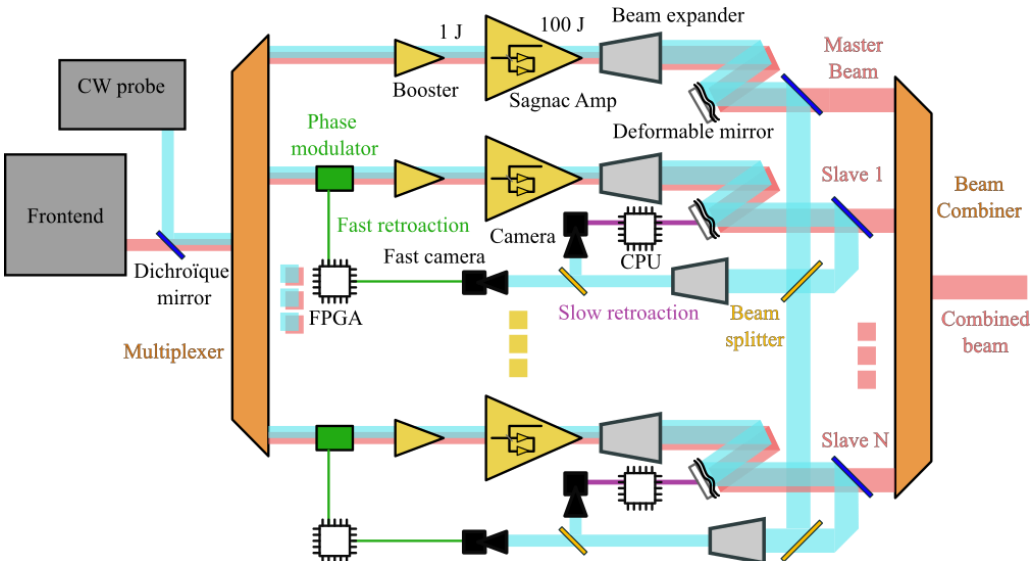

Figure 9: Conceptual design of a 1 kJ, 10 Hz laser based on passive and active CBC. The red laser line is the path of the amplified pulse, and the cyan is the path of the CW probe. A line (here the top one) can be considered as the reference master-beam-line; and all the slave sub-beam lines are locked into the master by two feedback loops, the slow one in purple and a fast one in green.

The design proposed in Fig. 9 is based on the MOPA architecture. The laser pulse is created in the front-end before adding the continuous probe. The chain then divides into 11-to-16 sub-beam lines (depending on the chosen separation/recombination technology). The sub-beam lines are pre-amplified by a booster to reach approximately 1 J. An amplifier based on a Sagnac architecture then amplifies the beam up to 100 J. The beam is subsequently expanded and passes through adaptive optics before recombination. The probe is recovered just before recombination; one of the sub-beam lines is chosen as the master, and the others as slaves, locked to the master. For this, an interference pattern is created with fringes for wavefront analysis using shearing interferometry. A camera analyses the differential wavefront between the slave sub-beam line and the master. It loops back to the deformable mirror to correct static and slow fluctuations of the chain as well as the pre-compensated part. Another faster camera analyzes the piston (a line-scan camera is sufficing) and can perform a high-speed piston phase loop with a fast actuator placed upstream of the chain. Currently, piezoelectric actuators (up to tens of kilohertz) and electro-optic modulators (several hundred megahertz) are available and can provide several λ of dynamic range correction.

5. Conclusion

The pursuit of an "ideal" laser source for inertial confinement Fusion applications has led to significant advancements in high-energy laser development. This study has explored the potential of a kilojoule-class system capable of operating at 10 Hz repetition rate, leveraging spatial CBC techniques to meet the demanding requirements of ICF and IFE. The use of CBC, both passive and active, has been demonstrated as a viable approach to achieving the necessary energy levels and repetition rates.

Passive CBC has been shown to be relatively easy to implement for a scale-up of a factor of two compared to straightforward methods, making it suitable for achieving energy levels of approximately 100 J. We experimentally demonstrated that this method is particularly effective in managing gain saturation and is well-suited for combining beams in the absence of correlation between subsequent pulses. However, extending passive CBC to more than one

recombination introduces significant complexity, making active CBC a more pertinent option for achieving higher energy levels.

Active CBC offers the capability to merge multiple beams that traverse different paths and amplifiers, allowing for greater scalability in the number of combinable sources. We proposed a complete architectural scheme capable of meeting all the challenging requirements for ICF applications based on an experimental study. A diagnostic method was demonstrated to probe, in real-time, the differential wavefront and relative piston fluctuations of two sub-beam lines on the pumping time scale. Experimental results indicated that the primary perturbations are piston and tilt, occurring on the order of tens of kilohertz. Other aberrations were shown to be negligible during the pumping flash. These experiments enable us to propose several correction strategies. Design based on the MOPA architecture, with the laser pulse created in the front-end and subsequently divided into multiple (11-to-16, typically) sub-beam lines. These sub-beam lines are first pre-amplified and then further amplified using a Sagnac interferometer architecture. They are subsequently recombined using cross-referenced real-time adaptive optics and feedback loops to correct static and slow fluctuations, along with a fast feedback loop for piston management.

The proposed design leverages the strengths of both passive and active CBC techniques. Passive CBC is used to achieve reliable and efficient amplification in the initial stages, while active CBC is employed in the final amplification stage to ensure that no single amplifier needs to handle the final beam diameter. This approach addresses the slow cooling problems of large amplifiers and ensures that the system can operate at the required repetition rates. Reducing the maximum size of the amplifiers from 200 mm to 40 mm diameter opens the opportunity to use alternative materials that are more difficult to manufacture at large diameters. Transporting, imaging and diagnosing the smaller chain is also much simpler and cheaper, which should significantly reduce the overall cost of the machine. Last but not least, the CBC and the proposed scheme also allow for maintenance while the system is in operation, a significant advantage for a machine intended for continuous use required by the IFE.

The use of CBC techniques, both passive and active, offers a promising route to achieving the necessary energy levels and repetition rates. The proposed architectural scheme provides a robust and realistic foundation-compatible with the needs of continuous use and reduce machine cost for ICF powerplant. This architecture can also be recommended for high-energy lasers with scientific or industrial applications, as well as high-intensity systems such as multi-petawatt laser chains [37,38].

Funding. HORIZON-INFRA-2022-TECH-01 by the European Union, for the “THRILL” project, number 101095207. SESAME filières PIA by Bpifrance , for the “CRONOS” project, DOS0153845/00 and DOS0153842/00.

Disclosures. The authors declare no conflicts of interest.

Data availability. Data underlying the results presented in this paper are not publicly available at this time but may be obtained from the authors upon reasonable request.

References

1. H. Abu-Shawareb, R. Acree, P. Adams, *et al.*, (Indirect Drive ICF Collaboration), "Achievement of Target Gain Larger than Unity in an Inertial Fusion Experiment", Physical Review Letters, Vol. 132, Issue 6, 065102 (2024). DOI: 10.1103/PhysRevLett.132.065102
2. LLNL page, Achieving Fusion Ignition (posted April 11, 2025, during the IFE STAR conference). https://lasers.llnl.gov/science/achieving-fusion-ignition
3. S. P. Obenschain, R. Lehmberg, D. Kehne, *et al.*, "High-energy krypton fluoride lasers for inertial fusion," Physics of Plasmas, Vol. 13, Issue 5, 056303 (2006). DOI: 10.1063/1.2178221

4. D. Eimerl, E. M. Campbell, W. F. Krupke, *et al.*, "StarDriver: A Flexible Laser Driver for Inertial Confinement Fusion and High Energy Density Physics," Journal of Fusion Energy, Vol. 33, pp. 476-488 (2014). DOI: 10.1007/s10894-014-9721-y
5. C. Labaune, D. Hulin, A. Galvanauskas, *et al.*, "On the feasibility of a fiber-based inertial fusion laser driver," Volume 281, Issues 15–16, August 2008, Pages 4075-4080, DOI:10.1016/j.optcom.2008.04.012
6. D. H. Froula, C. Dorrer, A. Colaïtis, *et al.*, "A future of inertial confinement fusion without laser-plasma instabilities," Physics of Plasmas, Vol. 32, Issue 5, 052703 (2025). DOI: 10.1063/5.0205809
7. Jean-Luc Miquel and Emmanuelle Prene, "LMJ & PETAL status and program overview," Nucl. Fusion 59 032005, DOI: 10.1088/1741-4326/aac343
8. P. D. Mason, S. Banerjee1, J. Smithet, *et al*., "Development of a 100 J, 10 Hz laser for compression experiments at the High Energy Density instrument at the European XFEL," High Power Laser Science and Engineering, Vol. 7, Issue 1, e1 (2019) (published online December 2018, but a foundational paper for the 100J, 10Hz system, and actively cited). DOI: 10.1017/hpl.2018.66
9. S. P. Hatchett et al., "The Mercury Laser System—An average power, gas-cooled, Yb:S-FAP based system with frequency conversion and wavefront correction," Journal of Fusion Energy, Vol. 28, pp. 195-202 (2009). DOI: 10.1007/s10894-008-9177-3
10. C. D. Orth, S. A. Payne, W. F. Krupke, "Diode-Pumped Solid State Laser Driver for Inertial Fusion Energy Power Plants," in Advanced Solid State Lasers, T. Fan and B. Chai, eds., Vol. 20 of OSA Proceedings Series (Optica Publishing Group, 1994), paper LT5
11. R. Chonion, J. M. Sajer, E. Bordenave, *et al*., "Multiphysics model of liquid-cooled Nd:phosphate split-slabs in large aperture optical amplifiers," Optics Express, Vol. 28, Issue 11, pp. 15792-15810 (2020). DOI: 10.1364/OE.390076
12. B. Rus, P. Bakule, R. Antipenkov, *et al.*, "ELI Beamlines lasers: status update," in High-power, High-energy Lasers, and Ultrafast Optical Technologies II, Proc. SPIE PC13532, PC135320E (June 3, 2025). DOI: 10.1117/12.3062737
13. Hamamatsu Photonics K.K. "Hamamatsu Photonics Announces Successful Output of 100‑ Joule Laser Pulses at a High Repetition Rate of 10 Hz." News Release, January 12, 2023. Hamamatsu Photonics. https://www.hamamatsu.com/jp/en/news/products-and-technologies/2023/20230112000000.html
14. M.Hanna, F. Guichard, Y. Zaouter, *et al.*, " Coherent combination of ultrafast fiber amplifiers," JOURNAL OF PHYSICS B-ATOMIC MOLECULAR AND OPTICAL PHYSICS 49, 6, 062004 (2016)
15. A. Klenke, M. Müller, H. Stark, *et al*., "Coherent Beam Combination of Ultrafast Fiber Lasers," in *IEEE Journal of Selected Topics in Quantum Electronics*, vol. 24, no. 5, pp. 1-9, Sept.-Oct. 2018, Art no. 0902709, DOI: 10.1109/JSTQE.2018.2808540.
16. L. Daniault, M. Hanna, D. N. Papadopoulos, *et al*., "Passive coherent beam combining of two femtosecond fiber chirped-pulse amplifiers," Opt. Lett. 36, 4023-4025 (2011)
17. L. Daniault, M. Hanna, L. Lombard, *et al.,* "Coherent beam combining of two femtosecond fiber chirped-pulse amplifiers," Opt. Lett. 36, 621-623 (2011)
18. P. Lebegue, J. De Sousa, C. Rapeneau, *et al.*, "Coherent combining of large-aperture high-energy Nd:glass laser amplifiers," High Power Laser Science and Engineering, Vol. 13, e4 (2025). DOI: 10.1017/hpl.2024.84
19. P. Lebegue, C. Rapeneau, D. Badarau, *et al.*, "Coherent combining of large-aperture high-energy Nd:glass laser amplifiers," Conference on Lasers and Electro-Optics/Europe (CLEO/Europe 2025), Technical Digest Series (Optica Publishing Group, 2025), Munich, Germany, June 23-27, 2025.
20. D.N. Papadopoulos, F. Friebel, A. Pellegrina, *et al.*, "High Repetition Rate Yb:CaF2 Multipass Amplifiers Operating in the 100-mJ Range" Invited in Selected Topics in Quantum Electronics, IEEE Journal of (Volume:21 , Issue: 1) (2015)
21. M. Kienel, M. Müller, S. Demmler, *et al.*, "Coherent beam combination of Yb:YAG single-crystal rod amplifiers," Opt. Lett. **39**, 3278-3281 (2014)
22. I. Fsaifes, L. Daniault, S. Bellanger, *et al.*, "Coherent beam combining of 61 femtosecond fiber amplifiers," Opt. Express 28, 20152-20161 (2020).
23. S. J. McNaught, C. P. Asman, H. Injeyan, *et al.*, "100-kW Coherently Combined Nd:YAG MOPA Laser Array," in Frontiers in Optics 2009/Laser Science XXV/Fall 2009 OSA Optics & Photonics Technical Digest, OSA Technical Digest (CD) (Optica Publishing Group, 2009), paper FThD2.
24. John Vetrovec, "Ultrahigh-Average Power Solid-State Laser," Conference: High Power laser Ablation Conference, Proceedings Volume 4760, High-Power Laser Ablation IV; (2002) doi:10.1117/12.482120
25. L. J. Waxer, M. J. Guardalben, J. H. Kelly, *et al.*, "The OMEGA EP High-Energy, Short-Pulse Laser System," in Conference on Lasers and Electro-Optics/Quantum Electronics and Laser Science Conference and

Photonic Applications Systems Technologies, OSA Technical Digest (CD) (Optica Publishing Group, 2008), paper JThB1

26. N. Jourdain, U. Chaulagain, M. Havlík, *et al.*, “The L4n laser beamline of the P3-installation: Towards high-repetition rate high-energy density physics at ELI-Beamlines”, Matter Radiat. Extremes 1 January 2021; 6 (1): 015401. https://10.1063/5.0022120
27. L. M. Frantz, J. S. Nodvik, “Theory of pulse propagation in a laser amplifier”, Journal of Applied Physics, 34(8), 2346–2349 (1963). https://doi.org/10.1063/1.1702744
28. M. Kienel, A. Klenke, T. Eidam, *et al.*, "Analysis of passively combined divided-pulse amplification as an energy-scaling concept," Opt. Express 21, 29031-29042 (2013)
29. C. Cui, Y. Wang, Z. Lu, *et al.*, "Demonstration of 2.5 J, 10 Hz, nanosecond laser beam combination system based on non-collinear Brillouin amplification," Opt. Express 26, 32717-32727 (2018)
30. R. Humblot, B. Stéphane, L. Meignien, *et al.*, "High fidelity phase conjugation in a stimulated Brillouin scattering cell at 122 J," Opt. Express 32, 47347 (2024).
31. J. B. Ohland, N. Lebas, V. Deo, *et al.*, Apollon “Real-Time Adaptive Optics: astronomy-inspired wavefront stabilization in ultraintense lasers.” High Power Laser Science and Engineering, Volume 13 , 2025 , e29. DOI: 10.1017/hpl.2025.16
32. J. P. Zou, A. M. Sautivet, J. Fils, *et al.*, "Optimization of the dynamic wavefront control of a pulsed kilojoule/nanosecond-petawatt laser facility," Appl. Opt. 47, 704-710 (2008)
33. M. Ahmad, M. Galletti, P. Oliveira, *et al.,* “Time-resolved thermally induced aberrations in a flash-lamp pumped Nd:Glass disk amplifier using a 2 × 2 position sensitive detector array”, Rev Sci Instrum. 2019 Dec 1;90(12):123106. DOI: 10.1063/1.5120388.
34. H. N. Yum, and M. S. Shahriar, “Pump–probe model for the Kramers–Kronig relations in a laser”, Journal of Optics, 12(10), 104018. (2010) DOI: 10.1088/2040-8978/12/10/104018
35. G. D. Goodno, C. Shih, and J. E. Rothenberg, "Perturbative analysis of coherent combining efficiency with mismatched lasers," Opt. Express **18**, 25403-25414 (2010)
36. M. Nourry-Martin, N. Fermon, C. Le Blanc, *et al.*, "Indirectly LED-pumped Nd:glass: potential for high energy laser facilities," Optica **12**, 311-314 (2025)
37. D. Wang and Y. Leng, "Simulating a four-channel coherent beam combination system for femtosecond multi-petawatt lasers," Opt. Express **27**, 36137-36153 (2019)
38. A. B. Nazîru, Ş. Popa , A-M. Lupu, *et al*., "Drift-free, 11 fs pulse delay stability in dual-arm PW-class laser systems”, High Power Laser Science and Engineering. 2024;12:e64. DOI: 10.1017/hpl.2024.54